The Journal of Chemical Physics ARTICLE scitation.org/journal/jcp

Distinguishing steric and electrostatic molecular probe orientational ordering via their effects on reorientation-induced spectral diffusion

Cite as: J. Chem. Phys. 154, 244104 (2021); doi: 10.1063/5.0053308
Submitted: 6 April 2021 • Accepted: 8 June 2021 •
Published Online: 23 June 2021

David J. Hoffman, Sebastian M. Fica-Contreras, Junkun Pan, and Michael D. Fayer[a)]

AFFILIATIONS

Department of Chemistry, Stanford University, Stanford, California 94305, USA

[a)]Author to whom correspondence should be addressed: fayer@stanford.edu. Telephone: 650 723-4446

ABSTRACT

The theoretical framework for reorientation-induced spectral diffusion (RISD) describes the polarization dependence of spectral diffusion dynamics as measured with two-dimensional (2D) correlation spectroscopy and related techniques. Generally, RISD relates to the orientational dynamics of the molecular chromophore relative to local electric fields of the medium. The predictions of RISD have been shown to be very sensitive to both restricted orientational dynamics (generally arising from steric hindrance) and the distribution of local electric fields relative to the probe (electrostatic ordering). Here, a theory that combines the two effects is developed analytically and supported with numerical calculations. The combined effects can smoothly vary the polarization dependence of spectral diffusion from the purely steric case (least polarization dependence) to the purely electrostatic case (greatest polarization dependence). Analytic approximations of the modified RISD equations were also developed using the orientational dynamics of the molecular probe and two order parameters describing the degree of electrostatic ordering. It was found that frequency-dependent orientational dynamics are a possible consequence of the combined electrostatic and steric effects, providing a test for the applicability of this model to experimental systems. The modified RISD equations were then used to successfully describe the anomalous polarization-dependent spectral diffusion seen in 2D infrared spectroscopy in a polystyrene oligomer system that exhibits frequency-dependent orientational dynamics. The degree of polarization-dependent spectral diffusion enables the extent of electrostatic ordering in a chemical system to be quantified and distinguished from steric ordering.

I. INTRODUCTION

The dynamics of condensed-phase chemical systems are often driven by the interplay of intermolecular electrostatic and steric interactions. The relationship between these forces produces the complex behavior of liquids with charged species, which has been well studied in electrolytic and ionic liquid systems.[1–5] These interactions also dictate the behavior of many macromolecular systems, particularly in biological substrate–enzyme binding[6–8] but also in the interactions of polymers and membranes with small molecules.[9–12] Despite the fundamental importance of these interactions, it is difficult to experimentally assess the relative contributions of electrostatic and steric forces on measured chemical dynamics.

This work provides a theoretical basis for distinguishing electrostatic and steric contributions to the orientational dynamics of a probe molecule using polarization-selective two-dimensional (2D) correlation spectroscopy. 2D correlation spectroscopy is a useful method for the study of the structures and dynamics of chemical systems.[13–17] A key observable in 2D spectroscopies is spectral diffusion. Spectral diffusion reports on the dynamics of a chemical system by measuring the time-dependent frequencies of embedded probe molecules across an inhomogeneously broadened absorption spectrum. The instantaneous frequency of a chromophore depends on its local environment. As the structures of the local environments evolve in time, each chromophore's frequency moves through the range of frequencies that compose the inhomogeneous spectrum. The dynamics of spectral diffusion can be characterized by the frequency–frequency correlation function (FFCF),

$$C(t) = \langle \delta\omega(t)\delta\omega(0)\rangle, \tag{1}$$

where $\delta\omega(t)$ is the instantaneous frequency of the chromophore at time t and the bracket indicates an ensemble average.

While a chromophore's frequency changes because the structure of its chemical environment evolves, it is also possible for a chromophore's frequency to vary because the chromophore itself moves.[18,19] On short time scales, the most significant chromophore motion is reorientation. The theory of reorientation-induced spectral diffusion[18–22] (RISD) describes how the reorientation of a chromophore affects its frequency, given a relationship between the instantaneous frequency of the chromophore, the orientation of the chromophore, and a vector field resulting from the environment (typically a local electric field).[18,19] After RISD is quantified, its effects on the FFCF can be accounted for to determine the component of the spectral diffusion that arises from the evolution of the local environment, which is termed structural spectral diffusion (SSD).[18] The effects of RISD have been seen and studied extensively in two-dimensional infrared (2D IR) spectroscopy,[18,19,21–27] but it has also been demonstrated in electronic excited state spectroscopy with dynamic Stokes shift measurements.[20]

RISD theory describes the polarization dependence of spectral diffusion measurements.[18,19] A schematic of the RISD effect is shown in Fig. 1(a). In a typical 2D experiment, the first two laser pulses "label" the initial frequency of a chromophore. The chromophore frequency is determined by the orientation of the probe molecule relative to a local electric field (green arrows in Fig. 1) and is represented by color in Fig. 1. The laser only labels chromophores that have projections of their transition dipoles along the polarization of the laser pulse [Fig. 1(a), filled distribution at $t = 0$]. The system then evolves in time. The chromophores will reorient [Fig. 1(a), curved arrows] and the chemical environments will structurally evolve. Both processes can cause the frequencies of the chromophores to change.

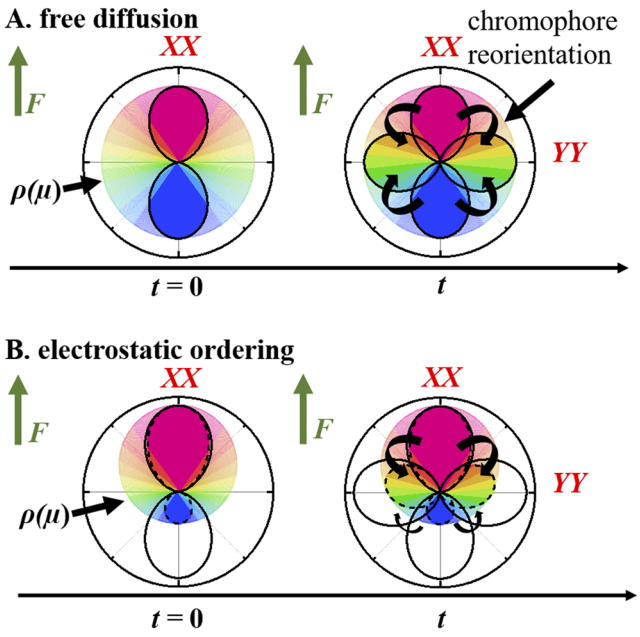

FIG. 1. (a) Schematic illustration of the RISD effect. A population of probe molecules is labeled at time zero (filled distribution), which is aligned with the polarization of the pump pulse. The color of the distribution reflects the probe molecules' frequencies due to their orientation relative to the electric field (green arrow). As time evolves, the probe molecules undergo orientational diffusion (curved arrows). The probe molecules that remain aligned with the initial pump polarization (vertical distribution) would have changed their frequency less than those that have rotated in the electric field and are probed with the perpendicular polarization (horizontal distribution). (b) If the electric field also induces ordering on the ensemble of probe molecules, then the RISD effect is enhanced. The initial probe molecules are both more likely to be aligned with the electric field at time zero and less likely to change their orientations. The distribution probed with parallel polarization changes frequency even less than in the free diffusion case, and the perpendicular polarization exhibits an even greater relative frequency change.

A third pulse ends the evolution period and gives rise to a fourth pulse, the vibrational echo. The heterodyne detected echo is the signal that reports both the initial and final frequencies of the chromophores. In effect, the third pulse initiates the read out of the final frequencies of the system for chromophores that were originally in the distribution at $t = 0$ and have a projection of their transition dipoles in the direction of the third pulse's polarization [Fig. 1(a), filled distributions at time t]. If the third pulse has the same polarization as the first two pulses and the echo is detected with this polarization [XXXX or "parallel" polarization; vertical distribution at time t in Fig. 1(a)], it will bias the measurement toward molecules that have undergone little reorientation in the local field, which results in a minimal frequency shift and a smaller RISD contribution to the spectral diffusion. If the third pulse and echo have polarizations orthogonal to the first pulses [XXYY or "perpendicular" polarization; horizontal distribution at time t in Fig. 1(a)], the signal will be biased toward molecules that have reoriented, resulting in a larger frequency shift and an increased RISD contribution to the spectral diffusion.

Despite the success of the RISD theory,[18–21,28] it is common to underestimate the degree of the spectral diffusion polarization dependence. While the most extreme departures have motivated the use of different mechanisms for polarization-dependent spectral diffusion,[21,29] generally these cases have been assigned to deviations from an assumption in the original RISD theory: coupling between the orientational dynamics of the chromophores and the structural dynamics,[23,24] heterogeneous orientational dynamics of the chromophores,[26] or electrostatic ordering of the probe molecules to their local electric fields.[22,25] The effect of electrostatic ordering may be particularly important in 2D IR spectroscopy, as IR probe molecules are often small and have large permanent dipole moments and the local electric fields experienced by the probe molecules can be quite large (on the order of GV/m).[30–32] The effects of the electrostatic ordering further decrease the degree of RISD seen in the parallel polarization while enhancing the RISD seen in the perpendicular polarization [see Fig. 1(b)].[22] The electrostatic ordering also produces restricted angular motion of the probe molecule analogous to steric confinement.

This work expands on previous numerical analysis of the effect of electrostatic ordering on RISD[22] by developing an analytic theory to describe the combined effects of electrostatic and steric confinement on polarization-dependent spectral diffusion dynamics. This combination results in a mild dependence of the chromophore's orientational dynamics on its frequency, which may provide an indicator that electrostatic ordering should be considered for a chemical system. The results show that there is a wide range of polarization-dependent RISD behaviors between the pure steric and electrostatic cases arising from the same orientational dynamics of the probe

molecules. The magnitude of the difference in measured spectral diffusion between the parallel and perpendicular polarizations is shown to depend on the degree of electrostatic ordering experienced by the molecular chromophore and provides an experimental measurement of this property. Additionally, key analytical results and approximations are produced, which match the existing numerical results in the literature for the case of pure electrostatic ordering. The theory demonstrates that such ordering could account for many of the quantitative differences between the standard RISD theoretical predictions[18,19] and experimental measurements.

The new RISD equations were applied to polarization-selective 2D IR spectra of the CN stretch of the long-lived vibrational probe phenyl selenocyanate in a low molecular weight polystyrene system. While the polarization dependence of spectral diffusion in these systems is significantly greater than that predicted by standard RISD theory,[18,19] the dependence was quantitatively described by taking into account electrostatic ordering. The relationship between the electrostatic order parameters measured with RISD and the results of first-order Stark shift[30–33] calculations are also considered. It was found that the degree of electrostatic ordering is in accord with the electric field determined by the Stark shift for the system.

II. BACKGROUND THEORY

A. Background theory of RISD

This section presents an overview of RISD as presented in the original publications by Kramer *et al.*,[18,19] which will be referred to as "standard RISD theory" throughout this work. In particular, the standard RISD theory involves a first-order Stark effect interaction, probe molecules with parallel transition and difference dipole moments, and no correlations between the orientations of the probe molecules and the local electric fields (no electrostatic ordering). Sections III and IV extend the RISD theory to include the combined effects of electrostatic ordering and steric hindrance on first-order Stark effect RISD. The main text considers probes with coincident transition, difference, and permanent dipole moments, while the supplementary material considers probes with non-coincident dipole moments.

In general, the experiments that report on spectral diffusion do so using polarized laser pulses to excite the molecular transition of interest. The probability of an interaction occurring between a molecular transition and the laser pulse is proportional to $\hat{\varepsilon}\cdot\hat{\mu}_T$, where $\hat{\varepsilon}$ and $\hat{\mu}_T$ are the unit vectors of the laser electric field and molecular transition dipole moment, respectively. The polarization-dependent FFCFs [Eq. (1)], obtained from third-order spectroscopy, are ensemble averages that are polarization-weighted for each light–matter interaction as follows:[19]

$$\langle\delta\omega(t)\delta\omega(0)\rangle_p = \frac{1}{I_p(t)}\left\langle(\hat{\varepsilon}_\alpha\cdot\hat{\mu}_T(t))^2\delta\omega(t)(\hat{\varepsilon}_\beta\cdot\hat{\mu}_T(0))^2\delta\omega(0)\right\rangle, \tag{2}$$

where $\hat{\varepsilon}_\alpha$ is the laser polarization vector at time t and $\hat{\varepsilon}_\beta$ is the polarization vector at time zero. $I_p(t)$ is a time-dependent, polarization-dependent normalization factor, defined as

$$I_p(t) = \left\langle(\hat{\varepsilon}_\alpha\cdot\hat{\mu}_T(t))^2(\hat{\varepsilon}_\beta\cdot\hat{\mu}_T(0))^2\right\rangle, \tag{3}$$

which is equivalent to the third-order signal intensity obtained in a pump–probe experiment.[34]

The standard RISD theory generally uses a first-order Stark effect interaction for the instantaneous frequency.[18,19] (RISD has also been derived for the second-order Stark effect[21] but is not considered in this work.) For the first-order Stark effect,

$$\begin{aligned}\delta\omega(t) &\propto \vec{F}(t)\cdot\hat{\mu}_D(t) - \langle\vec{F}\cdot\hat{\mu}_D\rangle\\ &\propto |\vec{F}(t)|(\cos(\theta_F(t)) - \langle\cos\theta_F\rangle),\end{aligned} \tag{4}$$

where F is the local electric field experienced by the probe molecule and θ_F is the angle between the electric field and the dipole moment difference vector μ_D (difference between the dipole moment in the ground and first excited states for the measured transition). In general, the difference dipole can have a different orientation from the transition dipole. The main text will consider the common case where the two vectors are parallel, while the supplementary material provides analogous results for the general case. To the lowest order, the RISD observables have a quadratic dependence on the angle between the two dipoles, so the uniaxial case is still a good approximation when the two vectors are nearly coincident.

If the time-evolution of the direction of the E-field is slow or comparable to the orientational relaxation of the probe molecule, Eqs. (2) and (4) can be combined and factored into a contribution from the reorientation of the probe molecule (RISD) and from structural evolution of the medium [structural spectral diffusion, $SSD(t)$],[18]

$$\begin{aligned}\frac{\langle\delta\omega(t)\delta\omega(0)\rangle_p}{\langle\delta\omega^2\rangle} &= \frac{1}{I_p(t)\langle\delta\omega^2\rangle}\left\langle\begin{matrix}(\hat{\varepsilon}_\alpha\cdot\hat{\mu}_T(t))^2(\cos\theta_F(t) - \langle\cos\theta_F\rangle)\\ \times(\hat{\varepsilon}_\beta\cdot\hat{\mu}_T(0))^2(\cos\theta_F(0) - \langle\cos\theta_F\rangle)\end{matrix}\right\rangle\\ &\quad\times SSD(t)\\ &\approx\left(\frac{R_p(t)\langle\cos^2\theta_F\rangle - \langle\cos\theta_F\rangle^2}{\langle\cos^2\theta_F\rangle - \langle\cos\theta_F\rangle^2}\right)\times SSD(t)\\ &= \tilde{R}_p(t)\times SSD(t),\end{aligned} \tag{5}$$

where $R_p(t) = \langle\cos\theta_F(t)\cos\theta_F(0)\rangle_p/I_p(t)\langle\cos^2\theta_F\rangle$ is the "intermediary" RISD component and $\tilde{R}_p(t)$ is the "observable" RISD component. As demonstrated in Eq. (5), the observable RISD is the term that is seen by polarization-selective spectral diffusion measurements. The intermediary RISD term, which does not account for a non-zero value of $\langle\cos\theta_F\rangle$, has useful conserved behaviors between analogous electrostatic and steric potentials that will allow the observable RISD to be more easily calculated (Sec. III B). Both $\tilde{R}_p(t)$ and $R_p(t)$ are normalized to 1. The approximation in the second line of Eq. (5) comes from estimating the cross terms in the ensemble average as $\left\langle(\hat{\varepsilon}_\alpha\cdot\hat{\mu}_T(t))^2(\hat{\varepsilon}_\beta\cdot\hat{\mu}_T(0))^2\cos(\theta_F(t))\right\rangle \approx I_p(t)\langle\cos\theta_F\rangle$, which is accurate within a few percent for all cases examined in this work. The approximation is exact in the isotropic case [$(\hat{\varepsilon}\cdot\hat{\mu}_T)^2 = 1/3$] or in the absence of electrostatic ordering [$\langle\cos\theta_F\rangle = 0$ and $\tilde{R}_p(t) = R_p(t)$].

Equation (5) contains two Stark order parameters $\langle\cos\theta_F\rangle$ and $\langle\cos^2\theta_F\rangle$, which appear in the definition of the observable RISD components. $\langle\cos\theta_F\rangle$ is the average Stark shift normalized to the

Stark coupling and corresponds microscopically to the net tendency of probe molecules to point toward the local electric fields they are experiencing. $\langle\cos^2\theta_F\rangle$ relates to the spectral linewidth from the Stark effect (i.e., variance = $\langle\cos^2\theta_F\rangle - \langle\cos\theta_F\rangle^2$) normalized to the Stark coupling and relates to the net tendency of probe molecules to be parallel to the local electric field.

Structural evolution of the medium can produce changes in the magnitude of the E-field, but if it randomizes the direction of the E-field on a time scale fast compared to orientational relaxation [i.e., SSD(t) decays to zero quickly compared to $\tilde{R}_p(t)$], then RISD is not observed. The RISD framework can also include "scalar" structural spectral diffusion as an additive component to Eq. (5),[18] but empirically most data appear to be well described entirely through vector coupling.

If the distribution of the electric fields and dipole moments are both globally isotropic and isotropic with respect to each other (i.e., no electrostatic ordering to the local field), Eq. (5) can be analytically evaluated to obtain the polarization-dependent RISD terms.[18,19] In the special case where $\mu_T = \mu_D$, this gives

$$R_{p,H}(t) = \tilde{R}_{p,H}(t) = \frac{C_1(t) + \frac{p}{5}(2C_1(t) + 3C_3(t))}{1 + pC_2(t)}, \tag{6}$$

where p is the polarization weighting ($p = 0$ for isotropic, +4/5 for XXXX, and −2/5 for XXYY) and $C_l(t) = \langle P_l(\hat{\mu}_T(t)\cdot\hat{\mu}_T(0))\rangle$ is the lth order Legendre polynomial orientational correlation function of the molecular transition dipole, which describes the orientational diffusion of the probe molecule's transition dipole. A more general case where $\mu_T \neq \mu_D$ has been previously examined in the case of free angular diffusion[20] and is summarized in the supplementary material.

$C_2(t)$ can be determined experimentally using polarization-selective pump–probe experiments and related techniques.[34,35] If the measured orientational relaxation is a single exponential decay, it determines D_m, the orientational diffusion constant. Then, the other $C_l(t)$ are determined using $C_l(t) = \exp(-l(l+1)D_m t)$. However, if the orientational relaxation is non-exponential (such as from wobbling-in-a-cone dynamics[36,37]), Eq. (6) can still be used, but a model of the non-exponential dynamics is required to construct $C_1(t)$ and $C_3(t)$. This has been previously presented using wobbling-in-a-cone dynamics[18] and heterogeneous dynamics.[26]

This work will focus on the effects of different angular potentials on the RISD correlation functions, such as from wobbling-in-a-cone dynamics or electrostatic alignment. The equilibrium distribution of probe molecule orientations to an angular potential, $V(\Omega)$, is given by a Boltzmann distribution,

$$\rho(\Omega) = \frac{\exp(-\beta V(\Omega))}{\int d\Omega\, \exp(-\beta V(\Omega))}, \tag{7}$$

with $\beta = 1/k_B T$ and Ω describing a probe molecule's orientation relative to a given coordinate frame. The angular potential V is a function of the orientation of the electric field and/or steric alignment vector. For free angular diffusion, this is simply $V(\Omega) = 0$, and for the wobbling-in-a-cone model that was previously examined analytically in the context of RISD,[36–38]

$$V(\Omega_H) = \begin{cases} 0, & \hat{\mu}_T\cdot\hat{H} \geq \cos\alpha \\ \infty, & \hat{\mu}_T\cdot\hat{H} < \cos\alpha, \end{cases} \tag{8}$$

where Ω_H describes the orientation of the molecular transition dipole, μ_T, relative to the orientation of the steric hard cone potential, $\hat{H}$, and α is the half-angle of the cone. Figure 2(a) illustrates these potentials relative to different electric field orientations. These diagrams show that the electric field orientation (dashed black arrows) sets the probe frequency [Eq. (4), color] but does not affect the shape of the probe's angular distribution [Eq. (7)] in either case.

To examine the effect of electrostatic alignment of probe molecules to the local electric field on the time dependence of the RISD components, a numerical Markov chain model similar to that developed by Ren and Garrett-Roe was employed.[22] The Markov chain model describes the orientational relaxation of a probe molecule in a given angular potential, $V(\Omega)$, as a biased random walk on a discretized unit sphere. A full description of the calculation can be found in the supplementary material. Using the Markov chain model, the analytic RISD results can be reproduced for cases without electrostatic ordering. Figure 2(b) shows that

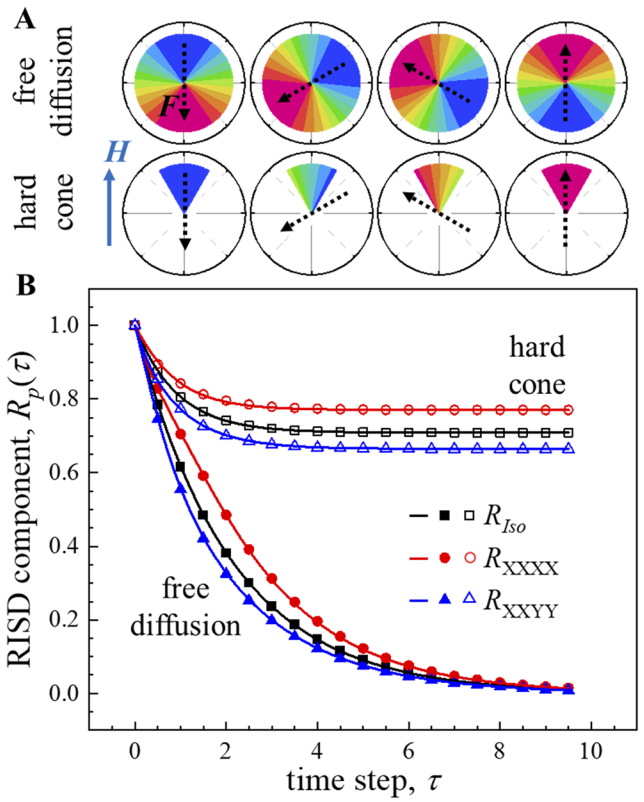

FIG. 2. (a) Probe orientation and frequency distributions for different electric field orientations for the case of free diffusion (top) and a wobbling-in-a-cone steric potential (bottom). The colors indicate the probes' frequencies. (b) The results of the Markov chain calculations[22] for the RISD components in the case of free diffusion (filled symbols) and with a wobbling-in-a-cone steric potential (open symbols) compared to the analytical theory [curves, from Eq. (6)].

the numerical calculations (symbols) quantitatively reproduce the analytic results[18,19] (curves) given in Eq. (6) for the case of free diffusion and wobbling-in-a-cone dynamics.

B. Analytic limits of the RISD terms

The RISD correlation function shown in Eq. (5) is a correlation function describing rotational diffusion of the probe molecule. Such correlation functions describing small-angle rotational diffusion can be expressed analytically as follows:

$$\langle A(\Omega(t))B(\Omega(0))\rangle = \int d\Omega(0) \int d\Omega(t) A(\Omega(t)) \times G(\Omega(t)|\Omega(0),t)B(\Omega(0))\rho(\Omega(0)), \quad (9)$$

where G is the Green's function describing a molecule in orientation Ω at time t given it was in orientation $\Omega(0)$ at time $t = 0$. The Green's function has a well-known expansion in terms of Wigner rotation matrices, which encodes the full time dependence of orientational diffusion.[20,39,40] The overall time dependence of an orientational correlation function in an angular potential is typically a sum of many exponential contributions, thus making it challenging to derive useful analytic results.[36,41] However, the initial and long-time behavior of these correlation functions are relatively tractable.[38]

The initial value of the correlation function goes as

$$\langle A(\Omega(0))B(\Omega(0))\rangle = \int d\Omega(0) A(\Omega(0))B(\Omega(0))\rho(\Omega(0)), \quad (10)$$

where the Green's function in Eq. (9) behaves as a Dirac delta function. Similarly, in the long-time limit the correlation function takes the value

$$\langle A(\Omega(t\to\infty))B(\Omega(0))\rangle = \langle A(\Omega)\rangle\langle B(\Omega)\rangle, \quad (11)$$

where the initial and final measurements are independent and both at equilibrium. In the case of an azimuthally symmetric potential, these expectation values can be written compactly as[38]

$$\langle A(\Omega)\rangle = \int d\Omega(t) A(\Omega(t))\rho(\Omega(t)) = \sum_l \frac{(2l+1)}{8\pi^2} S_l \int d\Omega(t) A(\Omega(t)) D^l_{00}(\Omega(t)), \quad (12)$$

where $D^l_{mn}(\Omega)$ is a Wigner rotation matrix and S_l is the order parameter (expectation value) for the lth Legendre polynomial $P_l(\cos\theta)$ in the angular potential $V(\Omega)$. The order parameters for the given azimuthally symmetric potential are then calculated as

$$S_l = \frac{1}{2}\int_0^\pi d\theta \sin\theta P_l(\cos\theta)\rho(\theta). \quad (13)$$

Any ensemble-averaged azimuthally symmetric observable can then be described in terms of the S_l order parameters.

The observables present in the RISD correlation function [Eq. (5)] can also be readily expressed in terms of rotation matrices.[20] Equation (12) can then be evaluated using Wigner rotation matrix identities for changing coordinate frames and integrations.[20,39,40] The calculations are further detailed in the supplementary material.

III. ELECTROSTATIC ORDERING

A. Initial and long-time values of the RISD components

This section will use the tools presented in Sec. II B to obtain analytic results for the RISD correlation functions in the presence of only electrostatic ordering. These results will then be expanded on in Sec. III B to obtain a full approximation for $\tilde{R}_p(t)$ under appropriate conditions. The effects of electrostatic ordering can be included by assigning the potential of[22,38,41]

$$V(\Omega_{FP}) = -V_F(\hat{\mu}_P\cdot\hat{F}) = -V_F D^1_{00}(\Omega_{FP}) \quad (14)$$

for a harmonic potential well depth, V_F, and the molecular permanent dipole moment, μ_P, with orientation Ω_{FP} relative to the local electric field. The depth of the potential is given by the product of the permanent dipole strength and the local electric field strength, $V_F = |\mu_P||F|$. V_F describes the tendency of the probe molecule to align to that local field, where a larger value of V_F indicates greater alignment. For simplicity, μ_P will also be assumed to be coincident with the transition and difference dipole moments. This case occurs frequently for small vibrational probe molecules. The general case is discussed in the supplementary material.

The top row of Fig. 3(a) illustrates this potential for various electric field orientations. Unlike the wobbling-in-a-cone case [Fig. 2(a)] or the steric harmonic case discussed in Sec. III B [Fig. 3(a), bottom row], both the angular confinement and frequency map change with changing electric field orientation. As discussed in Sec. II, it is difficult to get complete analytic expressions for the RISD results due to electrostatic alignment. However, important initial and final values of the RISD correlation functions are readily calculable in terms of S_l, the orientational order parameters calculated with Eq. (13) and summarized in Table I.

The Stark effect expectation values $\langle\cos\theta_F\rangle$ and $\langle\cos^2\theta_F\rangle$ used in the definition of the RISD component in Eq. (5) can be calculated in the electric field frame using Eq. (12),

$$\langle\cos\theta_F\rangle = S_1(\beta V_F), \quad (15)$$

$$\langle\cos^2\theta_F\rangle = \frac{1}{3} + \frac{2}{3}S_2(\beta V_F). \quad (16)$$

These values reflect how the overall frequency distribution changes in the presence of electrostatic ordering [Fig. 3(a), top row]. The values of $\langle\cos\theta_F\rangle$ and $\langle\cos^2\theta_F\rangle$ in the presence of the electrostatic ordering can then be markedly different from the free diffusion or pure steric hindrance cases, where their values are instead 0 and 1/3, respectively. As will be shown in Sec. III B, this is ultimately the most significant difference between electrostatic ordering and an equivalent steric potential for moderate V_F.

The long-time limiting behavior of the correlation functions for the probe orientational dynamics [Eq. (3)] and the RISD effect [Eq. (5)] can be found using Eq. (11). The angular restriction reported by the probe molecule's transition dipole (e.g., as measured by a complementary polarization-selective pump–probe experiment) tends toward the well-known result,[34,36]

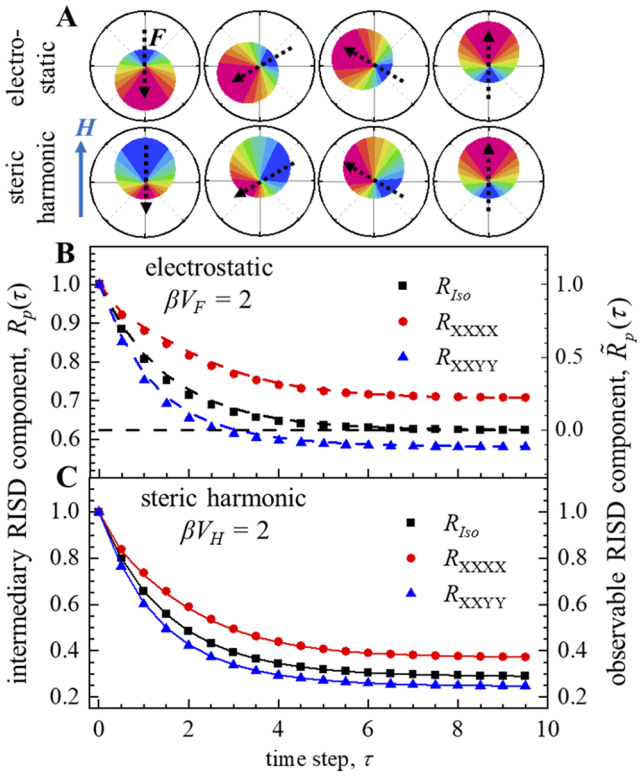

FIG. 3. (a) Probe orientation and frequency distributions for different electric field orientations for an electrostatic potential (top) and the equivalent steric harmonic potential (bottom). The results of the Markov chain model[22] for orientation in an electrostatic potential (b) and in an equivalent steric harmonic potential (c) with $\beta V = 2$ (symbols). Both potentials are constructed to produce identical orientational correlation functions. For the electrostatic potential, the observable RISD components (right-side scale) are shifted relative to the new average frequency (dashed black line). The isotropic curve goes to zero, while the XXXX and XXYY curves go to static offsets. The steric potential components more closely resemble the wobbling-in-a-cone result in Fig. 2, where all curves go to positive offsets. For (b), the dashed curves are the results of the analytic approximations, Eq. (26). For (c), the solid curves are the standard RISD theory[18,19] [Eq. (6)].

$$I_p(t \to \infty) = \frac{1}{9}\left(1 + p(S_2(\beta V_F))^2\right), \tag{17}$$

where p is the same polarization weighting as in Eq. (5) (0 for isotropic, +4/5 for XXXX, and −2/5 for XXYY). In the lab frame, the measured value of S_2 will tend toward zero in sufficiently fast systems due to the reorientation of the local electric fields. Using the results in Eqs. (16) and (17), the value of the intermediary RISD component $R_p(t)$ in a stationary electrostatic potential is

$$R_{p,F}(t \to \infty) = \frac{3{S_1}^2 + \frac{3p}{25}(2S_1 + 3S_3)^2}{\left(1 + p{S_2}^2\right)(1 + 2S_2)}, \tag{18}$$

where the S_l are again functions of βV_F. This result can be compared against the full RISD time dependence, which can be calculated using the Markov chain method[22] summarized in Sec. II A. Representative results of this calculation with $\beta V_F = 2$ are shown in Fig. 3(b), which reproduces the previous numerical results by Ren and Garrett-Roe.[22] In the isotropic case [$p = 0$, black points in Fig. 3(b)], Eq. (18) is equivalent to $\langle\cos\,\theta_F\rangle^2/\langle\cos^2\,\theta_F\rangle$ [black dashed line in Fig. 3(b)]. Plugging in R_p for the isotropic case into Eq. (5) shows that the observable isotropic electrostatic RISD component, $\tilde{R}_{Iso}(t)$, must then go to zero in the long-time limit [right-side scale, Fig. 3(b)]. This is in contrast to the isotropic RISD component in the presence of steric hindrance, which goes to a static offset at long time [Fig. 2(b), open black squares].

The parallel electrostatic RISD component [$p = +4/5$, red points in Fig. 3(b)] will then go to a positive offset, while the perpendicular RISD component [$p = -2/5$, blue points in Fig. 3(b)] will go to a negative offset. This arises because the initially excited probe molecule is more likely to be aligned with the electric field at time zero [Fig. 1(b)]. If the distribution is probed with the parallel polarization, the measurement will have comparably less contribution from molecules rotating into that direction, resulting in a bias toward molecules that have not moved and an even larger positive offset. By contrast, probing with the perpendicular polarization biases the measurement toward probe molecules that have moved more than average, resulting in a negative offset. As will be shown in Sec. III B, the entire time dependence of the electrostatic RISD components can be well approximated [Fig. 3(b), curves] using the limits and expectation values developed above.

TABLE I. Orientational order parameters for $\rho(\theta) \sim \exp(x\cos\theta)$.

l	$S_l(x)$
1	$\coth\,x - \frac{1}{x}$
2	$\frac{3x\,\coth\,x - x^2 - 3}{x^2}$
3	$\frac{(x^2+15)x\,\coth\,x - 6x^2 - 15}{x^3}$

B. Approximating the RISD time-dependence in the weak field limit

This section will use the results from Sec. III A to develop a full approximation of $\tilde{R}_p(t)$ in the presence of electrostatic ordering. Toward this end, the analogous steric potential to the electrostatic potential in Eq. (14) can be examined,

$$V(\Omega_{HP}) = -V_H(\hat{\mu}_P \cdot \hat{H}). \tag{19}$$

This form results in a steric harmonic potential that is analogous to the wobbling-in-a-cone potential given in Eq. (8) (for large V_H, $1 - \cos\alpha \approx 2/\beta V_H$) and is closely related to the "Gaussian cone" potential previously studied in the literature.[42] Significantly, the potential given by Eq. (19) generates Legendre orientational polynomial correlation functions, $C_l(t)$, that are quantitatively identical to the $C_l(t)$ from the electrostatic potential in Eq. (14) when $V_H = V_F$ [i.e., the shapes of the distributions in Fig. 3(a), top and bottom rows are the same besides orientation]. This means that the orientational diffusion of probe molecules in the potential given by Eq. (19) is the same as the reorientation of probe molecules dictated by Eq. (14), and the long-time behavior of $I_p(t)$ is still given by Eq. (17), with V_H instead of V_F.

The steric harmonic potential interacts with the polarization-weighted FFCF more like the steric wobbling-in-a-cone potential [Fig. 2(b), open symbols] than the electrostatic potential [Fig. 3(b)]. The similarity between the steric potentials can be seen by comparing the bottom row of Fig. 3(a) to the bottom row of Fig. 2(a). Importantly, the values of $\langle \cos \theta_F \rangle$ and $\langle \cos^2 \theta_F \rangle$ are 0 and 1/3, respectively, in both cases. The results of the steric harmonic potential with $\beta V_H = 2$ are shown in Fig. 3(c), where it can be seen that all three of the RISD components go to a positive offset at long time [again similar to the wobbling-in-a-cone potential in Fig. 2(b)]. The steric harmonic potential can also be quantitatively described by the analytic RISD equations given in Eq. (6) [Fig. 3(c), curves].

The general asymptotic behavior of the RISD components in the steric harmonic potential can be evaluated using Eq. (11),

$$R_{p,H}(t \to \infty) = \frac{{S_1}^2 + \frac{p}{5}\left(2{S_1}^2 + 3{S_3}^2\right)}{1 + p{S_2}^2}, \tag{20}$$

where S_l are here functions of βV_H. Equation (20) is also consistent with the asymptotic behavior of $C_l(t \to \infty) = {S_l}^2$ in Eq. (6) (however, this identity between the free-diffusion RISD expression and the steric RISD offset does not hold in the general case where $\mu_T \neq \mu_D$; see supplementary material).

While steric hindrance can be arbitrarily high for a given chemical system, the electrostatic ordering experienced by usual molecular dipole moments in typical local electric fields at moderate temperatures will correspond to $\beta V_F < 4$.[11] In these cases, the values of ${S_2}^2$ and S_3 will be very small and can be neglected in Eqs. (18) and (20). While the isotropic components in these two expressions differ by a factor of ~3, the anisotropic components [given by $R_{Aniso}(t) = R_p(t) - R_{Iso}(t)$] have a similar structure in this limit,

$$R_{Aniso,H}(t \to \infty) \approx \frac{4p}{10}{S_1}^2, \tag{21}$$

$$R_{Aniso,F}(t \to \infty) \approx \frac{12p/25}{1 + 2S_2}{S_1}^2. \tag{22}$$

Looking at the coefficients of Eqs. (21) and (22), it can be seen that the electrostatic case is 1.2× larger than the corresponding steric harmonic case. Furthermore, the S_2 term in the denominator of Eq. (22) will then make the electrostatic case slightly smaller and closer to the steric case. In this weak field limit, these anisotropic components are then nearly identical, i.e., $R_{Aniso,F}(t \to \infty) \approx R_{Aniso,H}(t \to \infty)$. Furthermore, this approximation illustrates that the enhanced polarization dependence in RISD caused by electrostatic ordering arises from the final step in Eq. (5) to generate the observable $\tilde{R}_p(t)$ terms [cf. Figs. 3(b) and 3(c), right-side scale].

Using the Markov chain calculations,[22] it can be shown that this approximation is excellent at all times within the weak field approximation [Fig. 4(a), symbols: electrostatic, curves: steric harmonic]. By construction, a steric system and an electrostatic system where $V_F = V_H$ will have identical Legendre orientational correlation functions, $C_l(t)$ [as the probe molecule orientational distributions in Fig. 3(a) all have the same shape]. Additionally, the RISD components of the steric harmonic cone can be described using the standard RISD theory presented in Sec. II A [Fig. 3(c)]. The anisotropic RISD components shown in Fig. 4(a) can be described in terms of the analytic expression in Eq. (6) for this case,

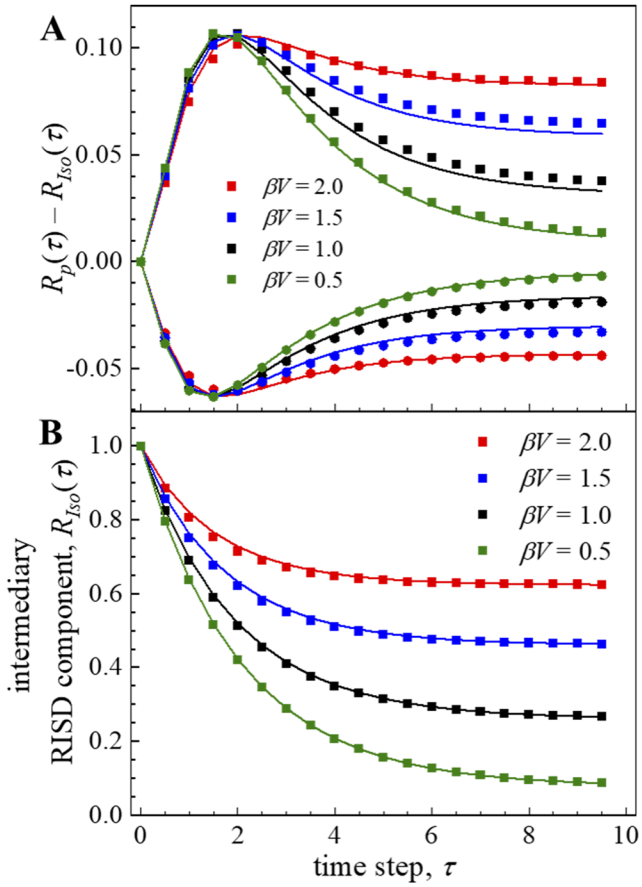

FIG. 4. (a) Differences between intermediary RISD components using the electrostatic and steric harmonic potentials (points and curves, respectively) for the various values of βV. Electrostatic results derived from the Markov chain model[22] and steric results derived from Eq. (6). Squares: R_{XXXX}, circles: R_{XXYY}. For the same value of βV, both cases have similar polarization dependences and identical orientational correlation functions. The RISD polarization dependence from electrostatic ordering can be well approximated by standard RISD theory[18,19] [Eq. (23)]. (b) The isotropic RISD component from the steric harmonic potential can be scaled and shifted using Stark order parameters to yield an approximation [curves, Eq. (25)] for the electrostatic R_{Iso} correlation function (squares).

$$R_{Aniso}(t) \approx \frac{C_1(t) + \frac{p}{5}(2C_1(t) + 3C_3(t))}{1 + pC_2(t)} - C_1(t). \tag{23}$$

As the polarization differences are conserved in the intermediary RISD components [Eqs. (21) and (22), Fig. 4(a)], the observable RISD components' polarization differences then depend entirely on the values of the Stark order parameters,

$$\tilde{R}_{Aniso}(t) = \left(1 - \frac{\langle \cos \theta_F \rangle^2}{\langle \cos^2 \theta_F \rangle}\right)(R_{Aniso}(t)). \tag{24}$$

The magnitude of the time-dependent RISD polarization difference between different measurements is dictated entirely by the steric

RISD results [Eq. (23)] and the values of the Stark effect order parameters [Eqs. (15) and (16)]. Therefore, the RISD polarization difference provides an experimental way to calculate the ratio of these two quantities.

Furthermore, if R_{Iso} can be analytically approximated for the electrostatic case in terms of known terms, the full time dependent electrostatic RISD components can be described analytically using $R_p(t) = R_{Iso}(t) + R_{Aniso}(t)$, which allows the structural spectral diffusion to be determined. As $C_1(t)$ is R_{Iso} in the pure steric case [Eq. (6)] and is known analytically, it will then be rescaled to have the same limiting behavior as the electrostatic R_{Iso}. Using $C_1(0) = 1$, $C_1(t \to \infty) = (S_1(\beta V_F))^2 = \langle \cos\theta_F \rangle^2$ (in the electrostatic case), and the result in Eq. (20), an approximate normalized R_{Iso} can be constructed after some algebra,

$$R_{Iso}(t) \approx (1-n)C_1(t) + n,$$
$$n = \frac{b}{a}\frac{(1-a)}{(1-b)}, \tag{25}$$

where $a = \langle \cos^2\theta_F \rangle$ and $b = \langle \cos\theta_F \rangle^2$ [Eqs. (15) and (16)]. The results of this approximation are shown in Fig. 4(b) for a variety of V_F. The approximate analytical R_{Iso} [curves, Eq. (25)] closely matches the numerically calculated R_{iso} (squares). Equation (25) can be combined with Eq. (23) to give a complete description of the RISD in the presence of electrostatic ordering in terms of only the Legendre orientational correlation functions and the Stark effect order parameters,

$$\tilde{R}_p(t) = \frac{(1-b)R_{p,H}(t) + \left(b - \frac{b}{a}\right)C_1(t) - b + \frac{b^2}{a}}{(1-b)\left(1-\frac{b}{a}\right)}, \tag{26}$$

where $R_{p,H}(t)$ is the RISD component in the absence of electrostatic ordering [Eq. (6)]. In Fig. 3(b), Eq. (26) (curves) can be compared to the Markov chain results (symbols), illustrating that this analytic expression can closely reproduce the numerical results from the literature for RISD in the presence of electrostatic ordering.[22] Additionally, in the limit that βV_F goes to 0, Eq. (26) becomes simply $R_{p,H}(t)$, restoring the original RISD result for free diffusion.

The above results provide a full analytic approximation for RISD in the case of electrostatic ordering in the weak field limit, which has been previously examined numerically.[22] The resulting expression in Eq. (26) introduces only a single new parameter, βV_F [via Eqs. (15) and (16)], beyond what is required for the standard RISD analysis[18,19] [Eq. (6)]. As will be shown in Sec. IV B, Eq. (26) can be applied without modification to the case of combined electrostatic and steric ordering.

IV. COMBINING ELECTROSTATIC AND STERIC ORDERING

A. Frequency-dependent orientational dynamics

In many physical systems, both steric and electrostatic effects will contribute to the dynamics experienced by a probe molecule. This section will focus on an observable consequence of their combined effects on the orientational dynamics of the chemical system, while Sec. IV B will examine the impacts on the RISD correlation functions. The resulting frequency-dependent orientational dynamics discussed below provide an experimental indicator of electrostatic effects on RISD.

A new angular potential, V, will be the sum of those described previously, $V(\Omega) = V_1(\Omega) + V_2(\Omega)$, i.e., the sum of the electrostatic potential [Eq. (14), top row of Fig. 3(a)] and the harmonic steric potential [Eq. (19), bottom row of Fig. 3(a)] or the sum of the electrostatic potential and the steric hard cone [wobbling-in-a-cone model, Eq. (8), bottom row of Fig. 2(a)]. These new combined potentials are illustrated in Fig. 5(a). This section will mainly look at the combined electrostatic/steric harmonic potential, as it has the additive property of

$$\begin{aligned} V(\Omega_{KP}) &= V_F\left(\hat{\mu}_P \cdot \hat{F}\right) + V_H\left(\hat{\mu}_P \cdot \hat{H}\right) \\ &= \hat{\mu}_P \cdot \left(V_F\hat{F} + V_H\hat{H}\right) \\ &= V_K \cos\theta_K, \end{aligned} \tag{27}$$

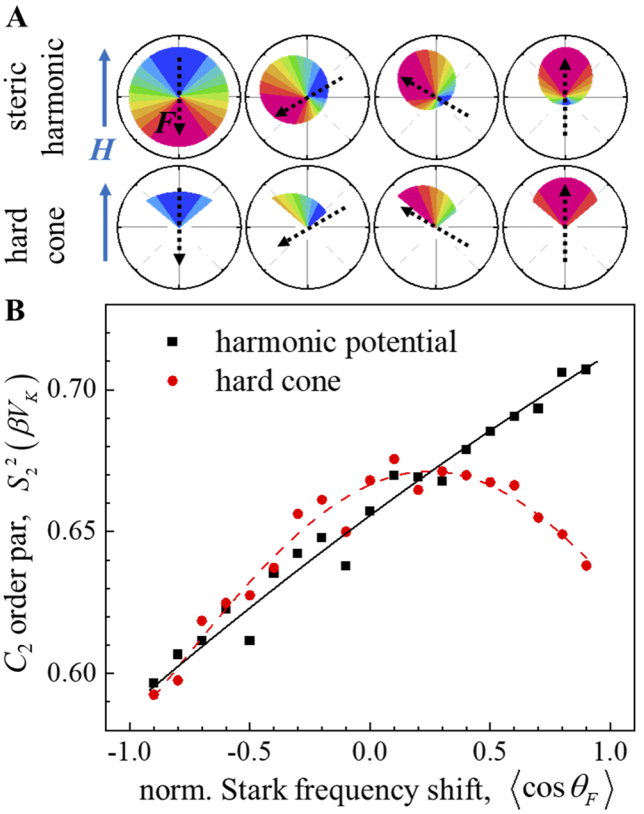

FIG. 5. (a) Probe orientation and frequency distributions for different electric field orientations for the combined electrostatic/steric harmonic and electrostatic/hard cone models. The shape and color of the distributions depend on the relative orientations of the contributions. (b) Calculations illustrating frequency-dependent orientational dynamics in the presence of both steric and electrostatic ordering for both steric potentials. As the steric and electrostatic potentials become more aligned, the Stark frequency shift [$\langle \cos\theta_F \rangle$ per Eq. (4)] will tend to increase and the orientational mobility of the probe molecule will tend to decrease (S_2 increases). Black parametric curve from Eqs. (28) and (29). Red curve is a guide to the eye.

with $V_K = \sqrt{V_F^2 + V_H^2 + 2V_F V_H \cos\gamma}$ and $\cos\gamma = \left(\hat{F}\cdot\hat{H}\right)$. The new combined potential K maintains azimuthal symmetry for all orientations of the component steric and electrostatic potentials, although the strength, V_K, and potential orientation vary with γ. By contrast, the hard cone combined potential is only azimuthally symmetric when the two component vectors are parallel.

If the steric potential can have orientations independent of the electric field direction, there will be sub-populations of probe molecules that cannot reach their equilibrium orientation relative to the electric field. Based on the Stark effect frequency relationship [Eq. (4)], different sub-populations then have different average frequencies based on their combined potential. Furthermore, these sub-populations will exhibit different orientational dynamics due to the differences in the strengths or geometries of the combined potentials. In general, the probe's orientational dynamics will be more restricted if the potentials overlap constructively ($\cos\gamma \sim +1$) and less restricted if the potentials overlap destructively ($\cos\gamma \sim -1$) [e.g., Fig. 5(a), top row]. Similarly, the frequency will be higher if the potentials are aligned (resulting in a larger $\langle\cos\theta_F\rangle$) and lower if the potentials are misaligned. Therefore, the combined steric and electrostatic potentials will result in frequency-dependent orientational dynamics of the probe molecules.

For the combined electrostatic/steric harmonic potential [Eq. (27)], the dependence of frequency and angular restriction can be worked out explicitly as a function of the angle between the two potentials, γ. The orientational restriction as measured by, e.g., a polarization-selective pump–probe experiment goes as

$$\langle P_2(\cos\theta_K)\rangle = S_2(\beta V_K(\gamma)), \tag{28}$$

while the frequency dependence from the Stark effect would go as

$$\begin{aligned}\langle\cos\theta_F\rangle &= \cos(\eta) S_1(\beta V_K(\gamma)) \\ &= \frac{V_F + V_H\cos\gamma}{V_K(\gamma)} S_1(\beta V_K(\gamma)),\end{aligned} \tag{29}$$

where η is the angle between the electrostatic potential and the new combined potential K. Equations (28) and (29) show that the frequency dependence is much more sensitive to the angle γ than the experimentally measured angular restriction. The combined potentials can also be numerically calculated by the Markov chain model, which gives results for the electrostatic/steric hard cone potential as well. For the steric harmonic potential calculation, $\beta V_F = 3$ and $\beta V_H = 15$. For the hard cone potential, $\beta V_F = 3$ and $\alpha = 33°$ were used.

Figure 5(b) illustrates the long-time behavior of the probe orientational dynamics as a function of $\langle\cos\theta_F\rangle$, which is related to the probe frequency [Eq. (4)], for both types of combined potentials. The expected overall trend can be seen, where the orientational dynamics become more restricted as the potentials become more aligned and $\langle\cos\theta_F\rangle$ increases. Additionally, frequency-dependent dynamics appear regardless of the exact shape of the steric potential, although the exact behavior differs between the steric harmonic (Fig. 5 black symbols) and hard cone potentials (red symbols). The steric harmonic potential combines cleanly, and the calculated points are described well by the parametric curve described by Eqs. (28) and (29) (black curve). The hard cone model, by contrast, demonstrates a local maximum at moderate $\langle\cos\theta_F\rangle$ (the red dashed curve is an aid to the eye). This effect arises from the electrostatic alignment causing the probe molecules to bunch up against the side of the hard cone potential [Fig. 5(a), bottom row], creating a higher degree of net alignment than if the cone was perfectly aligned with the electric field.

While Fig. 5 shows that frequency-dependent orientational dynamics are a possible consequence of combined electrostatic and steric potentials, it does not guarantee their presence. As shown by Eqs. (28) and (29), the relative angles of the component potentials affect the frequency dependence more than the degree of angular restriction. A high degree of steric ordering [e.g., $V_K(\gamma) \sim V_H$] or small degree of electrostatic ordering ($\beta V_F < 1$) greatly suppresses the effect. On the other hand, it is also not likely that this simple model is a complete description of frequency-dependent orientational dynamics, as it does not account for heterogeneity in the electric field strength or steric potential strength or shape.[11] These effects matter more when characterizing individual frequency subensembles (orientational relaxation in frequency resolved pump–probe experiments[11,12]) than when characterizing full ensemble behavior using 2D IR to obtain the FFCF. Figure 5 also demonstrates the dependence of frequency-dependent orientational dynamics on the shape of the component potentials, making it extremely challenging to characterize experimental frequency-dependent orientational dynamics using analogous calculations. Despite these caveats, the presence of frequency-dependent orientational dynamics supports consideration of combined electrostatic-steric influence on RISD, discussed below.

B. RISD in combined potentials in the weak field limit

This section will demonstrate the validity of the RISD approximation in Eq. (26) for systems with both electrostatic and steric effects. Unlike the frequency-dependent orientational dynamics discussed in Sec. IV A, spectral diffusion is typically characterized as an ensemble average of the entire line shape. Therefore, the resulting correlation functions involve integrating over all possible combinations of steric and electrostatic potential orientations. Within the constraints of the weak field limit that was considered in Sec. III B, this integration can be well approximated with a new effective angular potential. This new effective potential will then enable straightforward calculations of the expectation values and limiting behavior of the RISD functions for the combined electrostatic/steric harmonic potential introduced above.

The effective potential V_X is then defined as an integral of the combined potential [e.g., Eq. (27)] over all relative angles of the orientations of the component potentials, γ,

$$\exp(\beta V_X\cos\theta_{KP}) \sim \int d\gamma \sin\gamma \exp(\beta V_K(\gamma)\cos\theta_{KP} + \kappa\cos\gamma), \tag{30}$$

where κ is a parameter that describes the relative alignment between the steric and electrostatic potentials. For $\kappa = 0$, the two potentials are isotropic relative to each other, while large κ means that the two potentials generally have the same orientation. Relative to the lab frame, the distributions of probe molecules, electric fields, and steric potentials are still assumed to be isotropic. A quantitative description of the effective potential, V_X, can be found in the supplementary material, but it can be qualitatively understood using just the moments of $\cos(\eta)$, which describe the angles between the various combined potentials and the local electric fields.

The effective potential can then be used to approximate the integrals over γ for the expectation values described in Sec. IV A. For the angular restriction of the probe molecule [such as in Eq. (28)], this is simply

$$\langle\langle P_l(\cos\theta_K)\rangle\rangle \approx S_l(\beta V_X). \tag{31}$$

The average Stark shift [integral over Eq. (29)] and the second Stark order parameter are given by

$$\langle\langle \cos\theta_F\rangle\rangle \approx \langle\cos\eta\rangle S_1(\beta V_X), \tag{32}$$

$$\left\langle\left\langle \cos^2\theta_F\right\rangle\right\rangle \approx \frac{1}{3} + \frac{2}{3}\langle P_2(\cos\eta)\rangle S_2(\beta V_X). \tag{33}$$

These results can be seen to recover the simpler cases that were discussed in previous sections. In the case of a pure electrostatic potential ($V_X = V_F$ and $V_H = 0$), $\langle\cos\eta\rangle = \langle P_2(\cos\eta)\rangle = 1$. The above then simplifies to the results in Sec. III A. Similarly, a pure steric potential randomly oriented with respect to the electric field ($V_X = V_H$ and $V_F = \kappa = 0$) gives $\langle\cos\eta\rangle = \langle P_2(\cos\eta)\rangle = 0$, resulting in $\langle\langle\cos\theta_F\rangle\rangle = 0$ and $\left\langle\left\langle\cos^2\theta_F\right\rangle\right\rangle = 1/3$.

The new Stark effect order parameters in Eqs. (32) and (33) apply for the observable RISD equations [Eq. (5) or the approximation in Eq. (26)] when the steric hindrance persists long enough to affect the equilibrium distribution of probe frequencies. This condition requires the evolution of the steric hindrance to be essentially static on spectroscopically relevant time scales, i.e., in slowly evolving systems such as polymers. In systems with complex orientational dynamics, the final measured orientational restriction is likely the correct parameter to use, and the moments of $\cos(\eta)$ must be considered. If complete orientational randomization is achieved on the experimental time scale, the appropriate Stark effect parameters should be the simple Boltzmann parameters used in Sec. III A [Eqs. (15) and (16)].

Finally, the long-time behavior of the RISD correlation functions can be examined. Using the same approximations yields

$$R_{p,X}(t\to\infty) \approx \frac{\begin{pmatrix}(1+2\langle P_2(\cos\eta)\rangle)\left(25{S_1}^2 + p(2S_1+3S_3)^2\right)\\ +(2-2\langle P_2(\cos\eta)\rangle)\left(3p(S_1-S_3)^2\right)\end{pmatrix}}{25\left(1+p{S_2}^2\right)(1+2\langle P_2(\cos\eta)\rangle S_2)}, \tag{34}$$

where S_l are functions of βV_X. Equation (34) also simplifies to the pure electrostatic case [Eq. (18)] for $\langle P_2(\cos\eta)\rangle = 1$ and simplifies to the pure steric case [Eq. (20)] for $\langle P_2(\cos\eta)\rangle = 0$.

Equation (34) can be used to construct a weak-field approximation for the time-dependent RISD functions in the combined potential that is analogous to the approximation developed for the pure electrostatic case in Sec. III B. The first important scenario is when both V_F and V_H are small such that V_X is also small and ${S_2}^2$ and S_3 can be assumed to be approximately zero. The anisotropic RISD component [$R_{Aniso}(t) = R_p(t) - R_{Iso}(t)$] can then be approximated as

$$R_{Aniso,X}(t\to\infty) \approx \frac{\begin{pmatrix}4(1+2\langle P_2(\cos\eta)\rangle)\\ +3(2-2\langle P_2(\cos\eta)\rangle)\end{pmatrix}}{1+2\langle P_2(\cos\eta)\rangle S_2}\frac{p{S_1}^2}{25}. \tag{35}$$

The numerator can vary from 1.2× to 1×, the value of the pure steric case, $R_{Aniso,H}$ [Eq. (21)], for $\kappa > 0$, and the true values will again tend to be closer for moderate $S_2(\beta V_X)$. This result suggests that the same time-dependent approximation [Eq. (23)] applies for the combined potential as well. After approximating the isotropic RISD function $R_{Iso}(t)$ with Eq. (25) using the Stark effect order parameters in Eqs. (32) and (33), the full RISD time-dependent function can again be estimated using Eq. (26).

The second important weak-field case is when V_H is large but V_F is small, and the orientation of the steric potential is not highly correlated with the electrostatic potential. In this case, $V_X \sim V_H$ and is large enough that Eq. (35) is a poor approximation. However, $\langle P_2(\cos\eta)\rangle \sim 0$, so the RISD offset for the polarization-weighted and isotropic components can be described by the pure steric case in Eq. (21), which immediately implies that Eq. (6) describes the RISD time dependence. Unlike the true pure steric case, it is still possible for there to be an average Stark shift, $\langle\langle\cos\theta_F\rangle\rangle > 0$ [Eq. (32)], as $\langle\cos\eta\rangle$ is much more sensitive to electrostatic contributions than $\langle P_2(\cos\eta)\rangle$. The fully normalized RISD function can still be represented using Eq. (26).

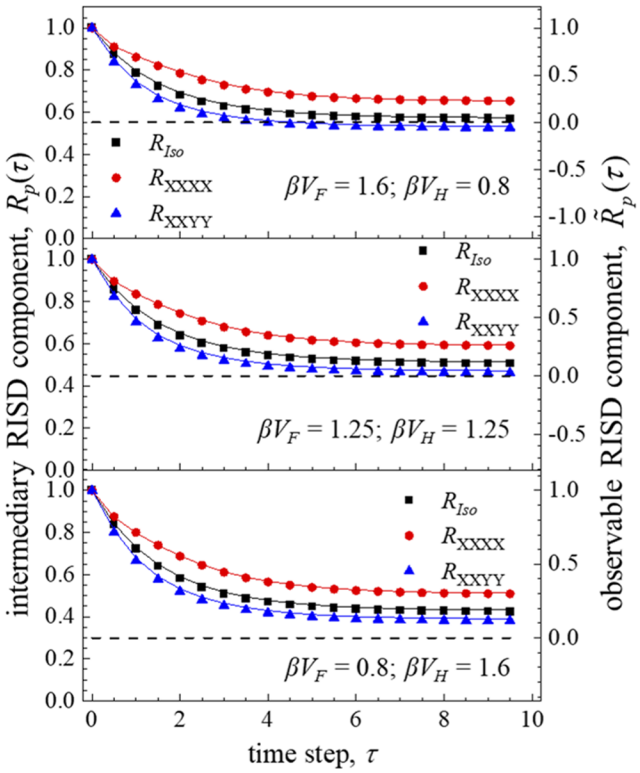

FIG. 6. Markov chain results for RISD components in the presence of both steric and electrostatic ordering (symbols). Each case has the same orientational correlation functions as the cases shown in Fig. 3 ($\beta V_X \approx 2$). In all cases, the calculated values closely match the analytic approximation in Eq. (26) (solid curves). For the corresponding observable RISD (right-side scale), the differences between polarization components (intercepts on the right-side axis) increase (bottom to top) as more electrostatic ordering is added. The differences between polarization components enable the degree of electrostatic ordering to be determined.

Example RISD correlation functions for combinations of steric potentials and harmonic potentials are shown in Fig. 6. The probe molecule has the same orientational dynamics in each of the cases shown and the cases illustrated in Fig. 3 ($\beta V_X \approx 2$). Through the combination of steric and electrostatic potentials, a continuous range of polarization-dependent spectral diffusion is possible for the same orientational dynamics observed with a polarization-selective pump–probe experiment. Considering the observable RISD components [Eq. (13), right-side scale of Fig. 6], the differences between different RISD polarization components increase with increasing electrostatic contribution until it reaches the purely electrostatic case illustrated in Fig. 3(b). Reducing the electrostatic contribution will similarly decrease the polarization differences until the purely steric case [Fig. 3(c)] is reached. Therefore, the degree of polarization difference measured experimentally reports on the overall degree of ordering of the probe molecule by the local electric field [Eq. (24)]. Significantly, all of the dynamics can still be described using the analytic approximations developed in Sec. III B [curves in Fig. 6, from Eq. (26)], indicating that the RISD approximation is valid in the case of combined electrostatic and steric dynamics as detailed in this section.

V. EXAMPLE APPLICATION TO 2D IR OF A PROBE MOLECULE IN A POLYSTYRENE OLIGOMER

The new RISD approximations were applied to a chemical system that displays strongly polarization-dependent spectral diffusion dynamics. Ultrafast IR experiments on small vibrational probe molecules embedded in polymers have displayed substantial frequency-dependent orientational dynamics measured with polarization-selective pump–probe experiments.[11,12] The frequency dependence is prominent even for oligomers with chains that are only a few units long. As discussed in Sec. IV A, this indicates that steric effects and possibly electrostatic effects may be needed to describe the system's spectral diffusion. The results of IR polarization-selective pump–probe and polarization-selective 2D IR experiments on the CN stretch of phenyl selenocyanate (PhSeCN, Sigma-Aldrich) in very low molecular weight polystyrene oligomer systems with five monomer units (Mw 580, Agilent) are shown in Fig. 7. Representative 2D spectra can be found in the supplementary material. The experimental methods used to acquire the data are identical to those described previously for high molecular weight polymeric systems,[11,12] and a complete description of the low Mw polystyrene oligomer system will be the subject of a future publication.

The PhSeCN/polystyrene oligomer system exhibited analogous strongly frequency-dependent orientational dynamics that have been previously reported for high molecular weight polystyrene.[12] The anisotropies [$r(t) = 0.4\, C_2(t)$] are shown in Fig. 7(a) for three frequencies across the inhomogeneously broadened CN stretch absorption spectrum. For nitriles such as PhSeCN, a larger electric field causes the frequency of the nitrile stretch to decrease.[30–33] Figure 7(a) shows that a larger average field correlates with more restricted orientational dynamics as demonstrated by a decrease in the amplitude of the rapid decay component of the biexponential decay occurring on an ~10 ps time scale. Similar behavior was derived in Sec. IV A.

However, the degree of frequency dependence seen in this system is much greater than can be reasonably obtained with the model

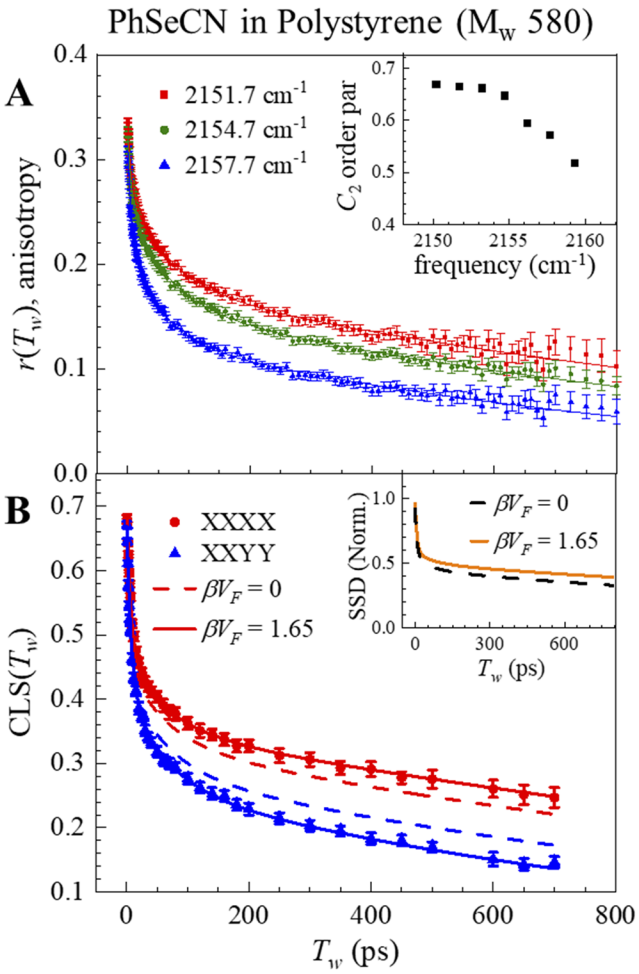

FIG. 7. (a) The frequency-dependent orientational dynamics of PhSeCN in a low MW polystyrene oligomer. The frequency dependence suggests that a combined electrostatic/steric model should be employed. Inset: frequency-dependent order parameter of $C_2(t)$, illustrating a much greater degree of frequency-dependent orientational dynamics than can be obtained with the model calculations [Fig. 5(b)]. (b) The polarization-dependent CLS decay data (symbols) of the same system. The standard RISD model[18,19] (dashed curves) systematically underestimates the polarization difference of the data. Using the combined electrostatic/steric model, the experimental data can be described quantitatively (solid curves). Inset: the structural spectral diffusion determinations, showing more correlated structural dynamics when electrostatic ordering is included although the difference is small.

presented in this work. Using Eqs. (28) and (29), $V_H \sim V_F \sim 10$, which would correspond to extremely strong local fields.[11] The frequency-dependent order parameter of $C_2(t)$ after the fast first diffusive process [Fig. 7(a), inset] can be compared to the results of the model calculation in Fig. 5(b). The much greater range spanned in Fig. 7(a) likely arises from correlated heterogeneity in the steric restriction experienced by probe molecules and local electric field strengths,[11,12] which is not accounted for by the model in this work. In particular, a distribution of electrostatic and steric component potential strengths (V_F and V_H, respectively), which are positively

correlated with each other (larger V_H coincides with larger V_F), could explain the observed trend.

The polarization-dependent center line slope (CLS) analysis reports on the polarization-dependent FFCF that is described by the RISD theory [symbols, Fig. 7(b)].[43,44] To avoid the effects of polarization-dependent motional narrowing, the CLS decays are first converted to the FFCF before the RISD equations are applied.[28] The RISD fit curves can then be converted back to CLS decays for comparison to the experimental data [curves, Fig. 7(b)].

The polarization-dependent CLS curves for the CN stretch of PhSeCN in polystyrene were first analyzed using the standard RISD equations[18,19] [Eq. (6)]. As the CLS observable is dominated by the center frequencies of the line shape,[27] a frequency-weighted $C_2(t)$ was constructed, which ultimately closely resembled the anisotropic curve at the line center of 2156 cm^{-1}. This multiexponential $C_2(t)$ curve was then described using the wobbling-in-a-cone model,[18,36,37] which allows the corresponding $C_1(t)$ and $C_3(t)$ to be constructed for use in Eq. (6). The RISD equations are then applied by performing a global fit of the FFCF for both polarizations with the various $C_l(t)$ held constant, and the parameters describing the structural spectral diffusion (SSD) allowed to float. The results of this procedure are the dashed lines in Fig. 7(b). As can be seen, this calculation systematically underestimates the observed polarization dependence in the CLS, which again suggests that electrostatic ordering may be impacting this system.

The approximate RISD equations with electrostatic ordering were then employed. The experimental data were fit to the analytic expression developed in Sec. III B [Eq. (26)]. The Stark effect order parameters were assumed to follow from the Boltzmann distribution [Eq. (14)] with potential depth V_F. The angle between the measured transition and permanent dipole moments for the PhSeCN nitrile stretch is ~15°,[45] which is sufficiently near collinearity that $\langle \cos^2 \theta_F \rangle$ and $\langle \cos \theta_F \rangle^2$ can reasonably be determined using Eqs. (15) and (16) (see the supplementary material). Additionally, possible steric effects on the Stark parameters as discussed in Sec. IV B appear to be negligible at equilibrium [curves in Fig. 7(a) tend to zero]. As before, all of the $C_l(t)$ were fixed during fitting, while the SSD parameters and the βV_F parameter contained in the Stark order parameters were allowed to float. The resulting fits using this procedure are shown as the solid curves in Fig. 7(b). The fit was found to describe the experimental data exceedingly well, with a resulting value of $\beta V_F = 1.65$. Fit residuals can be found in the supplementary material. At all times, the SSD shows more structural correlation than predicted using the standard RISD equations,[18,19] as more of the experimentally measured decay arises from RISD effects. However, the overall time dependence of the SSD was otherwise not strongly impacted by electrostatic effects (see inset). Similarly, the value of βV_F is too small to significantly impact the observed orientational dynamics shown in Fig. 7 (especially at short times) and cannot solely explain the frequency-dependent orientational dynamics.[11]

The value of the electrostatic potential depth, βV_F, can be compared to a similar value determined from the solvatochromism experienced by the probe molecule in the polystyrene matrix. Using the vibrational Stark effect parameters previously determined from the solvatochromism of PhSeCN,[11,32] the 2156 cm^{-1} absorption center frequency corresponds to an electric field of 0.63 ± 0.13 GV/m. As PhSeCN has a permanent dipole moment of ~4 D,[45] this corresponds to an estimated value of βV_F of 2.0 ± 0.4 at room temperature, which is within error of the value of 1.65 obtained in the RISD analysis. A nearly coincident value between the measured RISD βV_F and the estimated βV_F from the Stark shift could indicate that the local electrostatic fields are slowly varying, and there are no anomalous correlations in the relative orientations of the component steric and electrostatic potentials [κ is small in Eq. (30)]. As these conditions are plausible for polystyrene oligomers, the similarity between the electrostatic ordering parameter and the linear Stark shift parameter provides additional support for the validity of the modified RISD fit. The combined electrostatic/steric RISD model provides an excellent description of the spectral diffusion of the PhSeCN/polystyrene system.

VI. CONCLUDING REMARKS

The theory of reorientation-induced spectral diffusion[18–22] was expanded to include the combined effects of steric and electrostatic ordering. These phenomena have previously been examined separately but have not been combined into a single framework. Using analytic and numerical methods, the effects of including both types of potentials were determined explicitly. Critically, it was found that the RISD components for simple probe molecules in a purely electrostatic potential or in the new combined potentials could be well approximated analytically in terms of Legendre polynomial orientational correlation functions describing the reorientation of the probe molecule and two order parameters describing the electrostatic ordering. These new results can be directly applied in fitting experimental data without performing lengthy numerical calculations.

By combining both a steric and electrostatic potential, it was found that a continuous range of behavior in the RISD polarization dependence can be observed for the same orientational dynamics measured using polarization-selective pump–probe experiments. The polarization dependence ranges from the smallest dependence (a pure steric potential) to the largest (pure electrostatic). These findings suggest that the degree of RISD polarization dependence can indicate the degree of electrostatic ordering experienced by a probe molecule present in a chemical system. Additionally, it was found that the presence of both electrostatic and steric potentials will result in frequency-dependent orientational dynamics, providing an experimental test for the combined effects. Application of the results presented here to the analysis of 2D IR data may be able to determine if the combined steric/electrostatic effects, as opposed to other phenomena, give rise to an anomalously large polarization dependence in spectral diffusion.

The results were applied to the polarization-dependent spectral diffusion seen in 2D IR experiments on the CN stretch of PhSeCN in a low molecular weight polystyrene oligomer. The PhSeCN/polystyrene system exhibits frequency-dependent orientational dynamics, which is suggestive of the combined electrostatic and steric ordering. While the standard RISD theory[18,19] systematically underestimates the polarization-dependent spectral diffusion, the new theory was able to quantitatively describe the experimental data. The resulting electrostatic potential depth was also found to be within error of an analogous parameter obtained from vibrational Stark effect spectral analysis of PhSeCN in polystyrene, providing an independent support of the method.

As many important chemical systems include both strong electric fields and substantial steric ordering, this modified theory of reorientation-induced spectral diffusion can be applicable to a wide class of materials. Ultimately, it enables additional structural information to be gathered from a chemical system by observing the magnitude of the polarization dependence of spectral diffusion in 2D IR experiments while also providing a more accurate determination of the structural dynamics of the chemical system itself.

SUPPLEMENTARY MATERIAL

See the supplementary material for the Markov chain model (S1), analytic calculations with arbitrary dipole moment orientations (S2), note on RISD time dependence with arbitrary dipole moment orientations (S3), approximating the effective potential V_X (S4), and representative 2D spectra and RISD fit residuals (S5).

ACKNOWLEDGMENTS

This work was supported by the Office of Naval Research by ONR (Grant No. N00014-17-1-2656). D.J.H. was, in part, supported by the U.S. Department of Energy, Office of Science, Office of Basic Energy Sciences under Contract No. DE-AC02-76SF00515.

DATA AVAILABILITY

The data that support the findings of this study are available from the corresponding author upon reasonable request.

REFERENCES

[1]E. W. Castner, J. F. Wishart, and H. Shirota, "Intermolecular dynamics, interactions, and solvation in ionic liquids," Acc. Chem. Res. **40**, 1217–1227 (2007).
[2]M. Z. Bazant, B. D. Storey, and A. A. Kornyshev, "Double layer in ionic liquids: Overscreening versus crowding," Phys. Rev. Lett. **106**, 046102 (2011).
[3]M. A. Gebbie, M. Valtiner, X. Banquy, E. T. Fox, W. A. Henderson, and J. N. Israelachvili, "Ionic liquids behave as dilute electrolyte solutions," Proc. Natl. Acad. Sci. U. S. A. **110**, 9674–9679 (2013).
[4]Y.-L. Wang, B. Li, S. Sarman, F. Mocci, Z.-Y. Lu, J. Yuan, A. Laaksonen, and M. D. Fayer, "Microstructural and dynamical heterogeneities in ionic liquids," Chem. Rev. **120**, 5798–5877 (2020).
[5]M. S. Kilic, M. Z. Bazant, and A. Ajdari, "Steric effects in the dynamics of electrolytes at large applied voltages. I. Double-layer charging," Phys. Rev. E **75**, 021502 (2007).
[6]A. Dean and D. Koshland, "Electrostatic and steric contributions to regulation at the active site of isocitrate dehydrogenase," Science **249**, 1044–1046 (1990).
[7]A. Warshel, "Electrostatic basis of structure-function correlation in proteins," Acc. Chem. Res. **14**, 284–290 (1981).
[8]A. Warshel and M. Levitt, "Theoretical studies of enzymic reactions: Dielectric, electrostatic and steric stabilization of the carbonium ion in the reaction of lysozyme," J. Mol. Biol. **103**, 227–249 (1976).
[9]G. Gotchev, T. Kolarov, K. Khristov, and D. Exerowa, "Electrostatic and steric interactions in oil-in-water emulsion films from pluronic surfactants," Adv. Colloid Interface Sci. **168**, 79–84 (2011).
[10]J. Hansing and R. R. Netz, "Hydrodynamic effects on particle diffusion in polymeric hydrogels with steric and electrostatic particle–gel interactions," Macromolecules **51**, 7608–7620 (2018).
[11]D. J. Hoffman, S. M. Fica-Contreras, and M. D. Fayer, "Amorphous polymer dynamics and free volume element size distributions from ultrafast IR spectroscopy," Proc. Natl. Acad. Sci. U. S. A. **117**, 13949–13958 (2020).
[12]S. M. Fica-Contreras, D. J. Hoffman, J. Pan, C. Liang, and M. D. Fayer, "Free volume element sizes and dynamics in polystyrene and poly(methyl methacrylate) measured with ultrafast infrared spectroscopy," J. Am. Chem. Soc. **143**, 3583 (2021).
[13]S. Park, K. Kwak, and M. D. Fayer, "Ultrafast 2D-IR vibrational echo spectroscopy: A probe of molecular dynamics," Laser Phys. Lett. **4**, 704–718 (2007).
[14]A. Ghosh, J. S. Ostrander, and M. T. Zanni, "Watching proteins wiggle: Mapping structures with two-dimensional infrared spectroscopy," Chem. Rev. **117**, 10726–10759 (2017).
[15]J. P. Kraack, *Multidimensional Time-Resolved Spectroscopy* (Springer, Cham, Switzerland, 2019), pp. 113–205.
[16]P. Hamm and M. T. Zanni, *Concepts and Methods of 2D Infrared Spectroscopy* (Cambridge University Press, 2011).
[17]T. N. Do, M. F. Khyasudeen, P. J. Nowakowski, Z. Zhang, and H. S. Tan, "Measuring ultrafast spectral diffusion and correlation dynamics by two-dimensional electronic spectroscopy," Asian J. Chem. **14**, 3992–4000 (2019).
[18]P. L. Kramer, J. Nishida, and M. D. Fayer, "Separation of experimental 2D IR frequency-frequency correlation functions into structural and reorientation-induced contributions," J. Chem. Phys. **143**, 124505 (2015).
[19]P. L. Kramer, J. Nishida, C. H. Giammanco, A. Tamimi, and M. D. Fayer, "Observation and theory of reorientation-induced spectral diffusion in polarization-selective 2D IR spectroscopy," J. Chem. Phys. **142**, 184505 (2015).
[20]J. E. Thomaz, P. L. Kramer, S. M. Fica-Contreras, D. J. Hoffman, and M. D. Fayer, "Reorientation-induced Stokes shifts caused by directional interactions in electronic spectroscopy: Fast dynamics of poly(methyl methacrylate)," J. Chem. Phys. **150**, 194201 (2019).
[21]C. H. Giammanco, P. L. Kramer, S. A. Yamada, J. Nishida, A. Tamimi, and M. D. Fayer, "Carbon dioxide in an ionic liquid: Structural and rotational dynamics," J. Chem. Phys. **144**, 104506 (2016).
[22]Z. Ren and S. Garrett-Roe, "Reorientation-induced spectral diffusion of non-isotropic orientation distributions," J. Chem. Phys. **147**, 144504 (2017).
[23]A. Tamimi and M. D. Fayer, "Ionic liquid dynamics measured with 2D IR and IR pump–probe experiments on a linear anion and the influence of potassium cations," J. Phys. Chem. B **120**, 5842–5854 (2016).
[24]R. Yuan and M. D. Fayer, "Dynamics of water molecules and ions in concentrated lithium chloride solutions probed with ultrafast 2D IR spectroscopy," J. Phys. Chem. B **123**, 7628–7639 (2019).
[25]Z. Ren, J. Kelly, C. P. Gunathilaka, T. Brinzer, S. Dutta, C. A. Johnson, S. Mitra, and S. Garrett-Roe, "Ultrafast dynamics of ionic liquids in colloidal dispersion," Phys. Chem. Chem. Phys. **19**, 32526–32535 (2017).
[26]C. A. Johnson, A. W. Parker, P. M. Donaldson, and S. Garrett-Roe, "An ultrafast vibrational study of dynamical heterogeneity in the protic ionic liquid ethylammonium nitrate. I. Room temperature dynamics," J. Chem. Phys. **154**, 134502 (2021).
[27]P. L. Kramer, C. H. Giammanco, and M. D. Fayer, "Dynamics of water, methanol, and ethanol in a room temperature ionic liquid," J. Chem. Phys. **142**, 212408 (2015).
[28]D. J. Hoffman and M. D. Fayer, "CLS next gen: Accurate frequency–frequency correlation functions from center line slope analysis of 2D correlation spectra using artificial neural networks," J. Phys. Chem. A **124**(28), 5979–5992 (2020).
[29]D. J. Hoffman, S. M. Fica-Contreras, and M. D. Fayer, "Fast dynamics of a hydrogen-bonding glass forming liquid: Chemical exchange-induced spectral diffusion in 2D IR spectroscopy," J. Chem. Phys. **150**, 124507 (2019).
[30]S. Bagchi, S. D. Fried, and S. G. Boxer, "A solvatochromic model calibrates nitriles' vibrational frequencies to electrostatic fields," J. Am. Chem. Soc. **134**, 10373–10376 (2012).
[31]L. J. G. W. Van Wilderen, D. Kern-Michler, H. M. Müller-Werkmeister, and J. Bredenbeck, "Vibrational dynamics and solvatochromism of the label SCN in various solvents and hemoglobin by time dependent IR and 2D-IR spectroscopy," Phys. Chem. Chem. Phys. **16**, 19643–19653 (2014).
[32]N. M. Levinson, S. D. Fried, and S. G. Boxer, "Solvent-induced infrared frequency shifts in aromatic nitriles are quantitatively described by the vibrational Stark effect," J. Phys. Chem. B **116**, 10470–10476 (2012).

[33]B. Błasiak, A. W. Ritchie, L. J. Webb, and M. Cho, "Vibrational solvatochromism of nitrile infrared probes: Beyond the vibrational Stark dipole approach," Phys. Chem. Chem. Phys. **18**, 18094–18111 (2016).
[34]A. Tokmakoff, "Orientational correlation functions and polarization selectivity for nonlinear spectroscopy of isotropic media. I. Third order," J. Chem. Phys. **105**, 1–12 (1996).
[35]H.-S. Tan, I. R. Piletic, and M. D. Fayer, "Polarization selective spectroscopy experiments: Methodology and pitfalls," J. Opt. Soc. Am. B **22**, 2009 (2005).
[36]G. Lipari and A. Szabo, "Effect of librational motion on fluorescence depolarization and nuclear magnetic resonance relaxation in macromolecules and membranes," Biophys. J. **30**, 489–506 (1980).
[37]G. Lipari and A. Szabo, "Model-free approach to the interpretation of nuclear magnetic resonance relaxation in macromolecules. 1. Theory and range of validity," J. Am. Chem. Soc. **104**, 4546–4559 (1982).
[38]S. Stallinga, "Effect of rotational diffusion in an orientational potential well on the point spread function of electric dipole emitters," J. Opt. Soc. Am. A **32**, 213 (2015).
[39]D. M. Brink and G. R. Satchler, *Angular Momentum*, 2nd ed. (Oxford University Press, Oxford, 1968).
[40]R. N. Zare, *Angular Momentum* (Wiley-Interscience, 1988).
[41]D. E. O'Reilly, "Solution of the rotational diffusion equation for a polar molecule in an electric field," J. Phys. Chem. **74**, 3277–3279 (1970).
[42]K. Kinosita, A. Ikegami, and S. Kawato, "On the wobbling-in-cone analysis of fluorescence anisotropy decay," Biophys. J. **37**, 461–464 (1982).
[43]K. Kwak, S. Park, I. J. Finkelstein, and M. D. Fayer, "Frequency-frequency correlation functions and apodization in two-dimensional infrared vibrational echo spectroscopy: A new approach," J. Chem. Phys. **127**, 124503 (2007).
[44]K. Kwak, D. E. Rosenfeld, and M. D. Fayer, "Taking apart the two-dimensional infrared vibrational echo spectra: More information and elimination of distortions," J. Chem. Phys. **128**, 204505 (2008).
[45]S. Millefiori and A. Foffani, "Dipole moments and rotational isomerism for organic thio- and selenocyanates," Tetrahedron **22**, 803–811 (1966).